

# Outer-sphere CO release mechanism in the methanol to syngas reaction catalyzed by a Ru-PNP pincer complex

Jiali Liu,<sup>a,b</sup> Raquel J. Rama,<sup>c,\*</sup> Tomás Cordero-Lanzac,<sup>c</sup> Robert Franke,<sup>a,b</sup> and Ainara Nova<sup>c,d,\*</sup>

<sup>a</sup> Evonik Oxeno GmbH & Co. KG, Paul-Baumann-Str. 1, 45772 Marl, Germany

<sup>b</sup> Lehrstuhl für Theoretische Chemie, Ruhr-Universität Bochum, 44780 Bochum, Germany

<sup>c</sup> Center for Materials Science and Nanotechnology (SMN), Department of Chemistry, University of Oslo, 0315 Oslo, Norway

<sup>d</sup> Hylleraas Centre for Quantum Molecular Sciences, Department of Chemistry, University of Oslo, N-0315 Oslo

## Abstract

Methanol can be used as a surrogate model for H<sub>2</sub> and CO in the synthesis of a large variety of chemicals. In this work, the mechanism for the methanol to syngas reaction catalyzed by a Ru-PNP pincer complex has been studied using DFT and CCSD(T) calculations with methanol and toluene as the solvent. In the proposed mechanism, the CO is directly released from the methyl formate byproduct, forming a Ru-OCH<sub>3</sub> intermediate. This reaction is preferred in toluene compared to methanol due to the lower polarity of the organic products and the lower stability of the Ru-alkoxy intermediates. This mechanism differs from previous proposals going through a Ru-CO<sub>2</sub>CH<sub>3</sub> intermediate. The computed Gibbs free energy barriers for the different mechanisms were compared to experimental data using a microkinetic model coupled to a liquid-vapor batch reactor model designed from reported experimental setups. After refining the organic reaction thermodynamics consistent with CCSD(T)/cc-pVTZ method corrections, only our proposed mechanism shows a good agreement with the experimental H<sub>2</sub> and CO formation. Our findings herein demonstrate the usefulness of microkinetic modeling to support reaction mechanisms by direct comparison of computational and experimental data. In addition, the proposed mechanism rationalises the decarbonylation reaction in a way that can be easily extended to other carbonyl substrates and acid-base catalysts.

## Introduction

Methanol, obtained from captured CO<sub>2</sub> and green H<sub>2</sub>, has the possibility to replace fossil fuels for energy storage, ground transportation, and raw materials for synthetic hydrocarbons.<sup>1,2</sup> This route has a high industrial potential due to the required reaction conditions and the relevance of methanol as a platform chemical. Methanol is a versatile organic solvent and is used as a feedstock in the production of fine and bulk chemicals, including polymers. As an example, methanol can be used as a surrogate molecule for H<sub>2</sub> and/or CO to synthesize a large variety of products containing alcohol, aldehyde, amine, amide, and sulfonamide functional groups.<sup>3-5</sup>

While the mechanism for the decomposition of methanol into H<sub>2</sub> and CO catalyzed by metallic surfaces has been thoroughly investigated,<sup>6-12</sup> fewer studies have explored this transformation on metal oxide and zeolite heterogeneous catalysts,<sup>13, 14</sup> even though this reaction plays a critical role in the conversion of methanol to hydrocarbons.<sup>15, 16</sup> Recently, the mechanistic similarity between heterogeneous and homogeneous catalysts in hydrogen transfer reactions has been reported, with particular interest in catalysts with Lewis acid-base pairs such as metal oxides, M-N bifunctional homogeneous catalysts, and frustrated Lewis pairs.<sup>17, 18</sup> This is a significant advance since the isolated active site in homogeneous catalysts facilitates studying their mechanism of action.

In 2021, the formation of syngas from methanol was achieved by Leitner's group using  $\text{RuH}(\text{CO})(\text{BH}_4)(\text{HN}(\text{C}_2\text{H}_4\text{PPh}_2)_2)$  and  $\text{MnBr}(\text{CO})_2(\text{HN}(\text{C}_2\text{H}_4\text{P}^i\text{Pr}_2)_2)$  complexes yielding a ratio of  $\text{CO}:\text{H}_2$  close to the stoichiometric 1:2.<sup>19</sup> In this work, two catalytic cycles were proposed: one for the decarbonylation of formaldehyde resulting from methanol dehydrogenation; and the other for the decarbonylation of methyl formate, which is produced by the reaction of formaldehyde with methanol. The computational study of this reaction has recently appeared in two different publications.<sup>20, 21</sup> In both studies, it was proposed that the reaction does not proceed by the decarbonylation of formaldehyde but only via methyl formate. The mechanism for the overall reaction consists of the following steps: (i) methanol dehydrogenation, (ii) methanol and formaldehyde coupling, (iii) methoxy alcohol dehydrogenation, (iv) and methyl formate decarbonylation (Figure 1). While the mechanism for many of these steps is similar in the two studies and has been proposed for other reactions, such as the aqueous methanol-reforming<sup>22, 23</sup>, the mechanism for the methyl formate decarbonylation step has some differences. In particular on the orientation of the  $\text{CH}_3\text{OC}=\text{O}$  fragment, resulting from the deprotonation of methyl formate by the Ru-nitrogen complex, which coordinates Ru by either the  $\text{C}=\text{O}$  group (**Path A**) or the  $\text{OCH}_3$  group (**Path B**). Despite this difference, both reactions yield the same  $\text{Ru}-\text{COOCH}_3$  intermediate (**4**). The energy barrier for both routes (**A** and **B**) was similar; however, they were obtained using different computational methods. In addition, it is difficult to correlate the computed energies with the experimental formation curves of  $\text{H}_2$  and  $\text{CO}$  obtained by Leitner, since several Ru intermediates participate in more than one catalytic cycle (Figure 1). Especially in these cases, microkinetic models are useful, offering the possibility to directly compare computational and experimental data and elucidate the role of intermediates.<sup>24-26</sup>

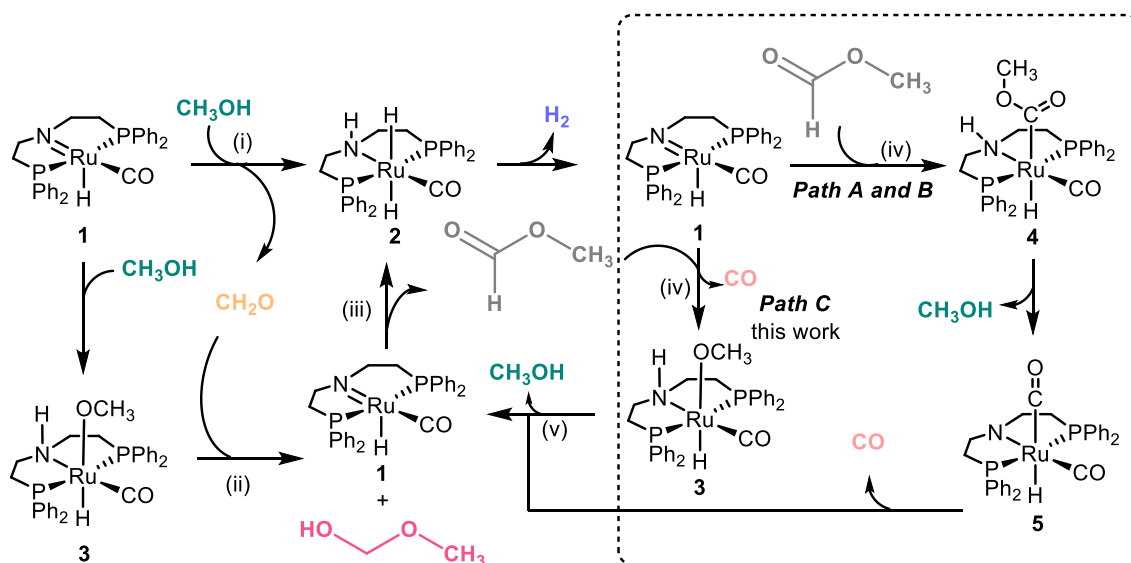


**Figure 1.** Reaction steps proposed computationally for the methanol to syngas reaction catalyzed by the Ru complex **1**: (i) methanol dehydrogenation, (ii) methanol and formaldehyde coupling, (iii) methoxy alcohol dehydrogenation, (iv) methyl formate decarbonylation and (v) catalyst recovery.

In this work, the same computational method was used to compute the complete reaction mechanism for the methanol-to-syngas reaction using methanol and toluene solvents. Further, these data were used to construct a microkinetic model, which was coupled with a Liquid-Vapor batch reactor model. Our results suggest that methyl formate decarbonylation, instead of forming intermediate **4** by pathways **A** or **B**, it yields the Ru-methoxy intermediate **3** by direct

CO release (**Path C**, Figure 2). This mechanism resembles the one proposed for decarbonylation reactions catalyzed by an organic base.<sup>27</sup> After refining the organic reaction thermodynamics consistent with CCSD(T)/cc-pVTZ method corrections, the new mechanism showed good agreement with the experimental data.

## Computational methods

Geometry optimization were carried out with the M06-L-D3<sup>28, 29</sup> functional, as implemented in the Gaussian16 software package.<sup>30</sup> Structures were fully optimized without any geometry or symmetry constraints with the double- $\zeta$  quality def2-SVP basis set.<sup>31, 32</sup> Vibrational frequencies were computed at the same level of theory to classify all stationary points as either saddle points (transition states, with a single imaginary frequency) or energy minima (reactants, intermediates and products, with only real frequencies). These calculations were also used to obtain the thermochemistry corrections (zero-point, thermal and entropy energies) at P = 1 atm and T = 298.15 K conditions. The energy of the optimized geometries was refined by single-point calculations with the M06-D3<sup>29, 33</sup> functional and triple- $\zeta$  quality def2-TZVP basis set.<sup>31, 32</sup> Solvent effects for methanol or toluene were included in all calculations using the SMD model.<sup>34</sup> The energies reported in the manuscript were obtained by adding the thermochemistry corrections to the refined potential energies. In addition, a correction of +/-1.9 kcal mol<sup>-1</sup> was applied to the Gibbs free energy change of reactions involving a change of molecularity for changing the standard state from the gas phase (1 atm) to solution (1 M).

## Results and discussion

**Decarbonylation of methyl formate:** The Gibbs Free energies obtained for the decarbonylation reaction of methyl formate catalyzed by **1** in methanol and toluene as solvent are shown in Figure 2. These solvents were selected because they were used in the experimental study of the methanol to syngas reaction.<sup>19</sup> In addition, **Path A** was previously studied in toluene.<sup>20</sup> Therefore, we were also interested in analyzing the effect of solvent in the reaction by comparing results in methanol, toluene and toluene/methanol (see Figure S1-S4 and Table S1-S4 in supporting information).

The two pathways previously proposed in the literature, **A** and **B**, start with the deprotonation of methyl formate by the amido ligand in **1** (**TS-1-6** and **TS-1-7**), followed by ligand rearrangement (**TS-6-4** and **TS-7-4**), yielding intermediate **4**. In methanol, the transition state with the highest energy in **Path A** is **TS-6-4**, where the CO<sub>2</sub>Me ligand changes its coordination from a  $k^1$ -O to  $\sigma^1$ -C, with an energy of 18.2 kcal mol<sup>-1</sup>. In **Path B**, the analogous TS (**TS-7-4**) was found at 16.6 kcal mol<sup>-1</sup> and has a similar energy than the deprotonation step via **TS-1-7** (16.5 kcal mol<sup>-1</sup>). In both cases, the formation of **4** is highly exergonic by 15.3 kcal mol<sup>-1</sup>. Methanol release from this intermediate has an energy barrier of 7.4 kcal mol<sup>-1</sup> (**TS-4-5**) and yields a dicarbonyl Ru intermediate (**5**), which has been experimentally detected.<sup>19</sup> This reaction and the CO ligand dissociation to recover catalyst **1** are both endergonic with energies of 7.3 and 19.4 kcal mol<sup>-1</sup>, which together yield an energy of 26.7 kcal mol<sup>-1</sup> for the overall process, suggesting that this is one of the limiting steps.

Calculations on **Path A** and **B** in toluene gave significantly different results. All intermediates and transition states increased in energy; in particular, **TS-6-4** in **Path A** went from 18.2 to 26.5 kcal mol<sup>-1</sup> in toluene. In addition, intermediate **7** in **Path B** could not be located as a minimum,

instead, it was found to be a transition state yielding the concerted deprotonation of methyl formate and C-OCH<sub>3</sub> bond cleavage (**TS-1-3-CO**, **Path C**). This step, with an energy barrier of 19.4 kcal mol<sup>-1</sup>, yields the methoxy intermediate **3**, which is involved in other steps of the methanol to syngas reaction (Figure 1). Energetically, **Path C** is not only lower than **A** by 7.1 kcal mol<sup>-1</sup>, but also prevents the formation of **4**, which is highly unfavorable for the reaction. In this case, methanol release from **3** has an energy barrier of 6.0 kcal mol<sup>-1</sup> and is endergonic by a similar energy. In addition, the formation of **5**, experimentally observed, is still possible by the addition of the released CO to the Ru complex **1**.<sup>19</sup>

The concerted decarbonylation reaction in toluene made us consider **Path C** also in methanol. In this case, instead of concerted, the CO elimination starts with the deprotonation of methyl formate via **TS-1-7** (as in **Path B**) followed by the C-OCH<sub>3</sub> bond cleavage (**TS-7-3**). From these two steps, the deprotonation has the highest energy barrier (16.5 kcal mol<sup>-1</sup>), and the CO release from intermediate **7** has an energy cost lower than 1 kcal mol<sup>-1</sup>. Comparing this result with **TS-7-4** in **Path B**, which is 5.5 kcal mol<sup>-1</sup> higher than **7**, indicates that **Path C** is also preferred in methanol.

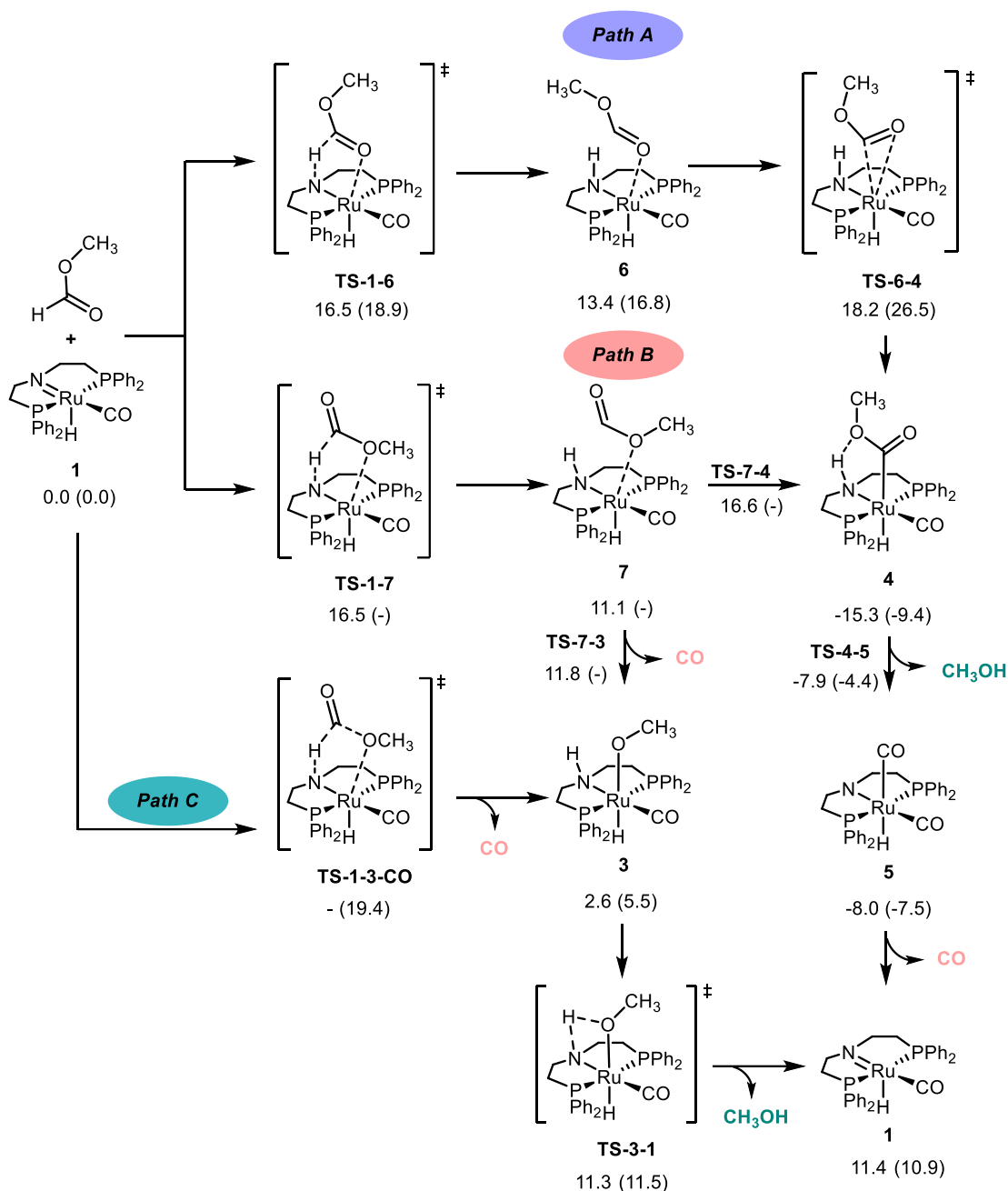


**Figure 2.** Gibbs Free energies (in kcal mol<sup>-1</sup>) in methanol, and toluene in parenthesis, for the decarbonylation of methyl formate via Paths A, B and C.

### Decarbonylation of formaldehyde:

The decarbonylation reaction following **Path C** can be understood as the fragmentation of methyl formate into a H<sup>+</sup>, CO and MeO<sup>-</sup> by the N-Ru base-acid pair. A similar fragmentation could occur with formaldehyde, in this case to H<sup>+</sup>, CO and H<sup>-</sup> (see Figure 3A). In methanol, the decarbonylation of formaldehyde by **Path C** follows a concerted mechanism with a higher energy barrier than that computed with methyl formate (21.1 kcal mol<sup>-1</sup> for formaldehyde and 16.5 kcal mol<sup>-1</sup> for methyl formate). In toluene, the reaction also follows a concerted mechanism, with formaldehyde having the lowest energy barrier (17.7 kcal mol<sup>-1</sup>) compared with methyl formate (19.4 kcal mol<sup>-1</sup>).

Analysis of the changes in the atomic charges of the H, CO, H/OCH<sub>3</sub>, and Ru-N fragments from reactants to the transition state (see Table 1 and Tables S5-S6) shows that electrons are transferred from H<sup>1</sup> to Ru-N in the case of formaldehyde, and to the CO fragment in methyl formate. One of the reasons for this difference is the more significant negative charge of CO in formaldehyde (-0.244 e) compared to methyl formate (0.061 e), in which the carbonyl group is more oxidized. It is probably the increase in the negative charge of CO in the case of methyl formate, which increases the polarity of the transition state, that makes the decarbonylation reaction preferred in methanol. In contrast, **TS-1-2-CO** is preferred in the less polar toluene solvent since the Ru-N fragment is less exposed to the solvent. For both substrates, H<sup>2</sup>/OCH<sub>3</sub> is slightly reduced.

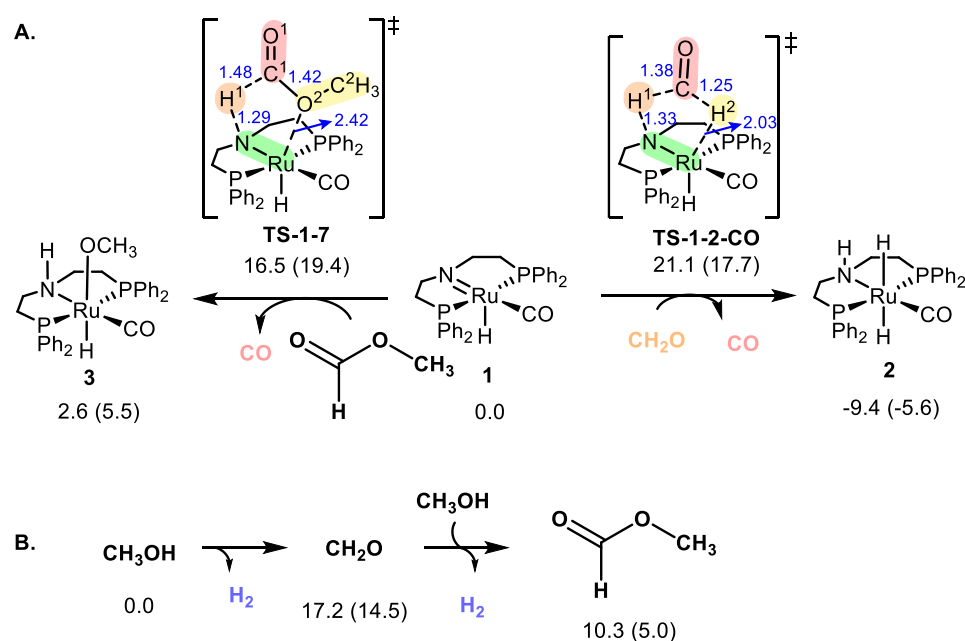


**Figure 3.** Gibbs Free energies (in kcal mol<sup>-1</sup>) in methanol, and toluene in parenthesis, for the decarbonylation of methyl formate and formaldehyde via Path C (A), and formation of these species from methanol (B). Blue numbers are optimized bond lengths in methanol solvent.

Table 1. NPA analysis of key atoms in structures optimized in methanol solvent.

Fragments	$\Delta q$ (1+CH <sub>2</sub> O – TS-1-2-CO)	$\Delta q$ (1+ HCOOCH <sub>3</sub> – TS-1-7)
H <sup>1</sup>	0.175	0.177
CO	-0.094	-0.244
H <sup>2</sup> or OCH <sub>3</sub>	-0.05	-0.044
RuN	-0.194	-0.006

When considering the decarbonylation energy barriers from both methyl formate and formaldehyde from **1**, they both seem reasonable and feasible under reaction conditions. However, the Gibbs free energy to form these intermediates from methanol ( $\Delta G$  in Figure 3B) should be added to the decarbonylation energy barriers ( $\Delta G^\ddagger$  in Figure 3A). In methanol, the formation energy of formaldehyde and methyl formate are 17.2 and 10.3 kcal mol<sup>-1</sup>, respectively. This means that overall, the global energy for the formaldehyde decarbonylation from methanol is significantly higher (38.3 kcal mol<sup>-1</sup>) than that for methyl formate (26.8 kcal mol<sup>-1</sup>). The same occurs in toluene, where the formation of formaldehyde and methyl formate are 14.5 and 5.0 kcal mol<sup>-1</sup>, respectively. Therefore, the overall energy barrier for the

decarbonylation of formaldehyde from methanol is 32.2 kcal mol<sup>-1</sup> and for methyl formate is 24.4 kcal mol<sup>-1</sup>. These energies suggest that, also by **Path C**, the methanol to syngas reaction follows the steps shown in Figure 1, including the formation of methyl formate instead of the direct decarbonylation of formaldehyde. However, formaldehyde can directly decarbonylate if used as the substrate. In addition, the energies found in methanol and toluene suggest that the decarbonylation process is slightly favored in toluene because of the preferred formation of methyl formate in this solvent. This result is consistent with recent experimental work reported using toluene as the main solvent for the methanol decarbonylation reaction.<sup>35</sup>

**Microkinetic model of the methanol to syngas reaction:** With the information previously described, we conclude that the formation of syngas from methanol is more likely to proceed via the formation of methyl formate and its decarbonylation by **Path C**. However, the full catalytic cycle is required to determine the key transition states of the reaction, the catalyst resting state and whether this mechanism agrees with the 2:1 molar ratio observed experimentally. Therefore, the complete mechanism was computed in methanol, toluene and toluene/methanol for comparison (see supporting information). The complete energy profile in methanol is shown in Figure 4.

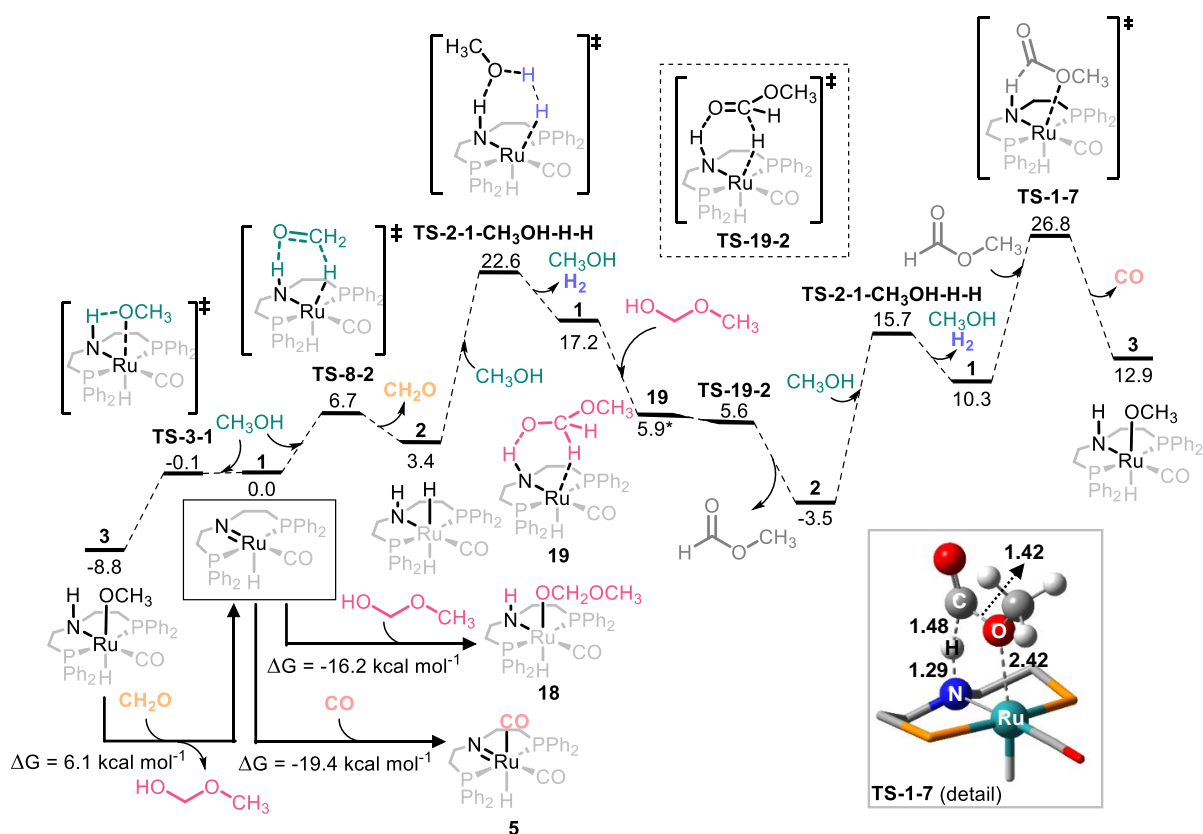


**Figure 4.** Gibbs Free profile (in kcal mol<sup>-1</sup>) in methanol for the methanol to syngas reaction catalyzed by **1**. \*Optimization in toluene and single point calculation in methanol.

The mechanism starts with the reaction of the Ru active catalyst **1** with methanol by two competitive pathways: methanol dehydrogenation yielding formaldehyde, and methanol deprotonation forming the Ru-OCH<sub>3</sub> **3** (Figure 4). This intermediate (**3**) reacts with formaldehyde yielding methoxymethanol, which, like methanol, can react with **1** leading to

methyl formate via dehydrogenation or **18** via deprotonation. From these products, only methyl formate can further react with **1** yielding CO via **Path C**. This decarbonylation reaction recovers the methoxy intermediate **3**, which needs to dissociate methanol to regenerate the active catalyst **1**. The formation of **1** from **2** is also needed after each dehydrogenation process and it is assisted by methanol. A detailed description of each step is included in the supporting information.

As the energy profile shows, while the highest transition states are well localized the overall energy barrier is difficult to predict because of competitive reactions involving the same intermediates. To solve this problem and directly compare our results with the experimental data from Leitner's work,<sup>19</sup> we built a microkinetic model with the computed energies in methanol. This model included calculations of the concentration of all species in solution and the gas phase. For this, we included liquid-vapor equilibrium in the reactor model, assuming the Henry constants for CO and H<sub>2</sub> in methanol reported by Wu et al.<sup>36</sup> and using Raoult's law to estimate the partial pressure of organic compounds in the gas phase. This assumption is valid due to the huge difference in concentrations between the solvent (methanol) and solutes. The consideration of the gas phase was critical in this reaction because a considerable amount of methanol would form the vapor phase under the reaction temperature (boiling point 64.7 °C). Unlike experimental observations, the model predicted a very fast formation of H<sub>2</sub>, while the CO formation was negligible (Figure 5A). A fast optimization of all energy values (Ru-species, organic molecules and transition states) showed that the free energy of organic molecules was those influencing the most the product formation. Therefore, we recomputed the energy of the organic molecules (methanol, CO, H<sub>2</sub>, methoxymethanol, formaldehyde and methyl formate) with a higher level of theory (CCSD(T)/cc-pVTZ). To our surprise, the thermodynamic values of the organic reaction at the CCSD(T) level were significantly different (Figure 5B), particularly the ΔG for the MeOH to H<sub>2</sub> and CO reaction. To implement these energy differences in our model, the energies for all organic intermediates, except MeOH and H<sub>2</sub>, were changed following the CCSD(T) corrections. Repeating the optimization protocol, adding a final correction of 1.2 kcal mol<sup>-1</sup> in the energy of H<sub>2</sub>, both H<sub>2</sub> and CO TON evolution predictions were significantly improved (Figure 5C), predicting the syngas composition of ca. 2.5:1 (H<sub>2</sub>:CO).

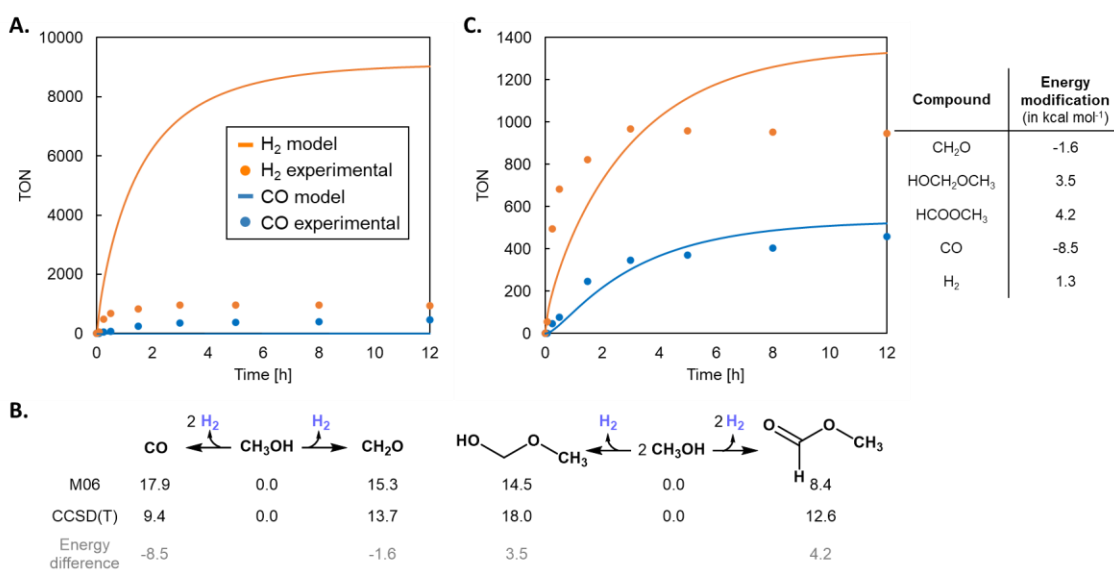


**Figure 5.** Comparison between the experimental TON of CO and H<sub>2</sub> produced versus time and modelled values of the path C (A) without modifications and (C) after the optimizations shown in the table. (B) Comparison of the thermodynamic values of the organic reactions at M06 and CCSD(T) levels.

After including the energy changes for the organic species, additional sensitivity analyses of all energy values were performed to evaluate the dependence of the TON and product distribution with all reaction intermediates (Figure 6 and S6). Figure 6 (and Figure S6) shows the comparison of H<sub>2</sub> and CO TON values after 12 h of reaction. As optimizations suggested before, the most substantial influence was shown by the organic molecules, namely methanol, CO and H<sub>2</sub>, which have a huge impact (in the  $\pm 2$  kcal mol<sup>-1</sup> range) over gas phase H<sub>2</sub> and CO production. The large effect indicates that the formation of products is limited by the reaction thermodynamics, which is highly endergonic ( $\Delta G = 17.9$  kcal mol<sup>-1</sup>). Formaldehyde has much less influence, as its formation and consumption via reaction with **3** have low energy barriers ( $\Delta G \leq 7$  kcal mol<sup>-1</sup>, see Figure 4 and S3). The catalyst intermediates that have the highest influence in the product formation are the Ru-OCH<sub>3</sub> intermediate (**3**) and **2-CH<sub>3</sub>OH**, in which the hydrogenated catalyst interacts with methanol. Not surprisingly, these are the catalyst resting states (see Figure 7). These species produce a small change in the TON when including an energy shift of -2 kcal mol<sup>-1</sup>. All other intermediates do not influence the TON unless changes are equal to or higher than -5 kcal mol<sup>-1</sup>, which leads to a decrease in the gas production. The increase of the TON cannot be achieved by changes in the catalyst because the reaction is limited by the methanol to syngas reaction thermodynamics.

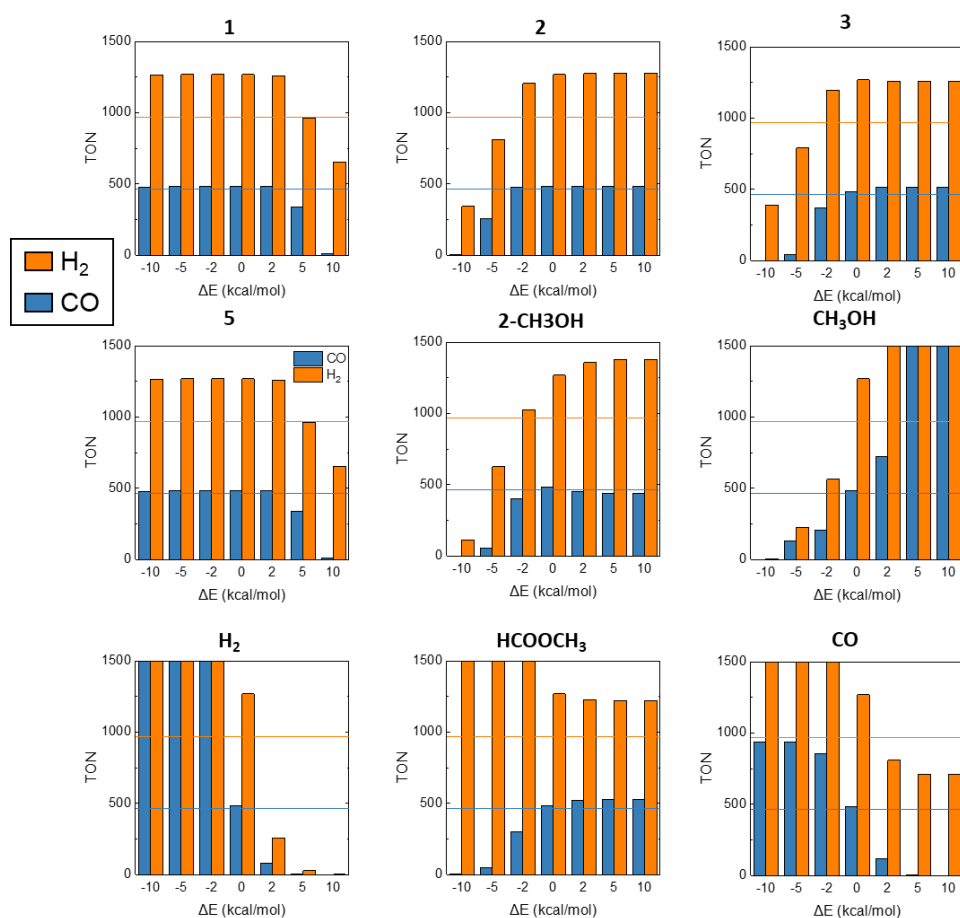


**Figure 6.** Sensitivity analysis of the free energy of the different intermediates in the TON of H<sub>2</sub> and CO after 12 h of reaction. Horizontal lines indicate observed TON values after 12 h by Leitner et al.<sup>19</sup>

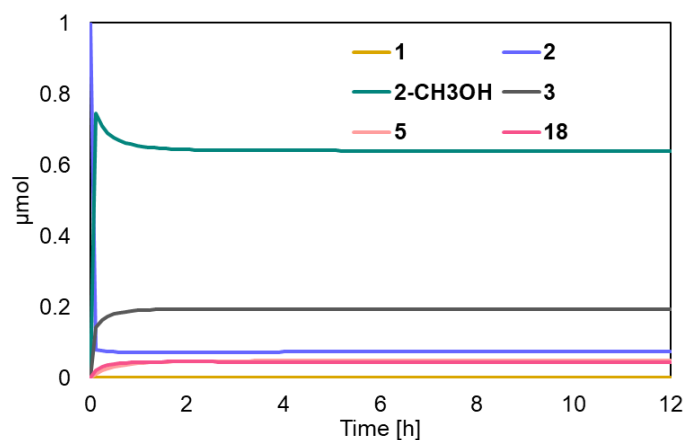


**Figure 7.** Evolution of the Ru-containing species over time during the reaction.

A microkinetic model for the methanol to syngas reaction was also performed including **Path A** instead of **C** for the decarbonylation of methoxyformate. **Path B** is very similar kinetically to **Path A**, so it was not included in the study. After the corrections for the organic species shown in Figure 5C, the sensitivity analysis over **Path A** showed that CO is only formed by destabilizing **4** in ca. 25 kcal mol<sup>-1</sup> or stabilizing CO in ca. 20 kcal mol<sup>-1</sup> (most likely a combination of both), which seems unfeasible. This result made us conclude that CO production might occur through the proposed **Path C**.

As methyl formate is proposed as the main source of CO formation, the reaction outcome using methyl formate as a reactant was also investigated. Qualitatively, the results predicted by the model and the **Path C** are similar to the experiments, with significantly higher production of CO than H<sub>2</sub> in this case.<sup>19</sup> However, the TON values predicted were higher than those observed in the experiments. We hypothesized that the solvent employed (*t*-amyl alcohol) might influence the outcome of the reaction because it could interact with the intermediate **1** in a similar manner to methanol (Figure 8A). To investigate our hypothesis, we computed the formation of complex **26** from **1** and *t*-amyl alcohol, which is thermodynamically favorable by ca. 5 kcal mol<sup>-1</sup>. This reaction was incorporated into the microkinetic model, and the inhibition effect of the solvent for CO production was studied (Figure 8B). Please note that this reaction does not have any impact on the previous results, as reactions were performed in pure methanol. Indeed, CO formation is clearly inhibited by the addition of the solvent, while the production of H<sub>2</sub> remains almost unchanged. Therefore, our results suggest that methyl formate and the solvent play a key role in the production of gas phase CO.

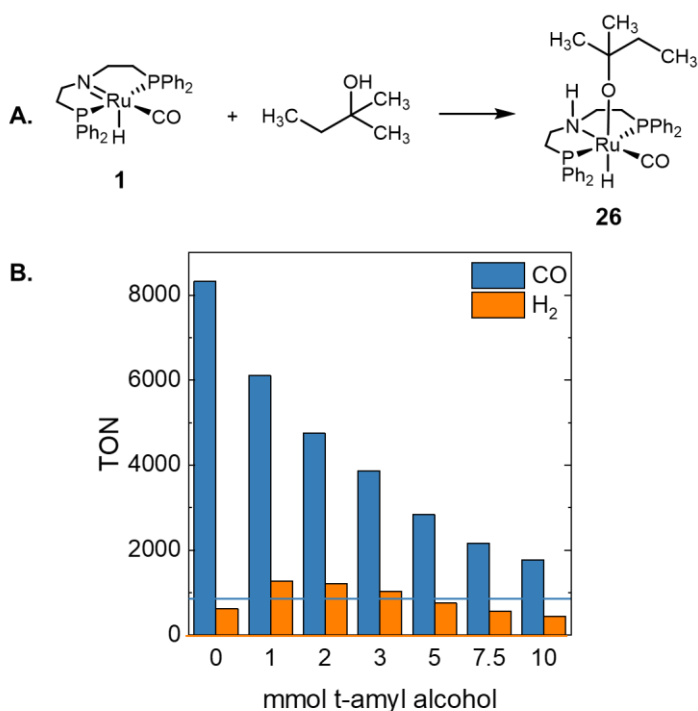


**Figure 8.** (A) Formation of complex **26** from complex **1** and *t*-amyl alcohol. (B) Analysis of the solvent concentration in the TON of CO and H<sub>2</sub> after 12 h of reaction using methyl formate as a substrate. Horizontal line indicates the observed TON values after 12 h by Leitner et al. using ca. 5 mmol *t*-amyl alcohol.<sup>19</sup>

## Conclusions

In this work, the methanol to syngas reaction mechanism was studied using DFT and CCSD(T) calculations and analyzed using microkinetic models. Our results show that the reaction does not go through a Ru-CO<sub>2</sub>CH<sub>3</sub> intermediate (**4**), as previously proposed.<sup>19</sup> Instead, the decarbonylation of methyl formate takes place by the direct liberation of CO by a stepwise (in methanol) or concerted (in toluene) reaction, yielding a Ru-OCH<sub>3</sub> intermediate (**3**). This mechanism is consistent with the fragmentation of methyl formate into H<sup>+</sup>, CO and OCH<sub>3</sub><sup>-</sup> fragments and is preferred over formaldehyde decarbonylation because of the higher stability of methyl formate compared to formaldehyde. This reaction is preferred in a non-polar solvent such as toluene over protic solvents such as methanol or *t*-amyl alcohol because it favors the formation of methyl formate (Figure 3B), and disfavors the formation of alkoxy Ru intermediates, such as **3** or **26**.

A sensitivity analysis considering variations in the free energy of all intermediates showed that the H<sub>2</sub>:CO ratio is highly influenced by the energy of the organic reactants, intermediates and products, which are highly influenced by the solvent and computational method. Instead, the energy of the Ru-containing intermediates needs to change by more than 5 kcal mol<sup>-1</sup> in most cases to impact the TON and product distribution. This information should be relevant for optimizing carbonylation reactions using methanol and other carbonyl-containing groups as CO-surrogate models. In addition, given the similar acid-base properties of the Ru-N in **1** with

some heterogeneous catalysts, the mechanistic information presented in this work may also be applied to heterogeneous catalysis.

## Acknowledgements

This project has received funding from the European Union's Horizon 2020 research and innovation programme under the Marie Skłodowska-Curie grant agreement No 859910 (J. L., R. F. and A. N.). R.J.R. acknowledge the Horizon Europe Framework Programme (HORIZON) 2021 under the Marie Skłodowska-Curie grant agreement 101061858. A.N. acknowledges financial support from the Research Council of Norway through the Centre of Excellence (no. 262695) and for its FRINATEK program (no. 314321) and the Norwegian Metacenter for Computational Science (NOTUR) for computational resources (project number nn4654k).

## References

- (1) Olah, G. A.; Goeppert, A.; Prakash, G. S. Chemical recycling of carbon dioxide to methanol and dimethyl ether: from greenhouse gas to renewable, environmentally carbon neutral fuels and synthetic hydrocarbons. *The Journal of organic chemistry* **2009**, *74* (2), 487-498.
- (2) Olah, G. A.; Goeppert, A.; Prakash, G. S. *Beyond oil and gas: the methanol economy*; John Wiley & Sons, 2011.
- (3) Kumar, A.; Daw, P.; Milstein, D. Homogeneous catalysis for sustainable energy: hydrogen and methanol economies, fuels from biomass, and related topics. *Chemical reviews* **2021**, *122* (1), 385-441.
- (4) Sivakumar, G.; Kumar, R.; Yadav, V.; Gupta, V.; Balaraman, E. Multi-Functionality of Methanol in Sustainable Catalysis: Beyond Methanol Economy. *ACS Catalysis* **2023**, *13* (22), 15013-15053.
- (5) Sordakis, K.; Tang, C.; Vogt, L. K.; Junge, H.; Dyson, P. J.; Beller, M.; Laurenczy, G. Homogeneous catalysis for sustainable hydrogen storage in formic acid and alcohols. *Chemical reviews* **2018**, *118* (2), 372-433.
- (6) Greeley, J.; Mavrikakis, M. Methanol decomposition on Cu (111): a DFT study. *Journal of Catalysis* **2002**, *208* (2), 291-300.
- (7) Baudais, F.; Borschke, A.; Fedyk, J.; Dignam, M. The decomposition of methanol on Ni (100). *Surface Science* **1980**, *100* (1), 210-224.
- (8) Kandoi, S.; Greeley, J.; Sanchez-Castillo, M. A.; Evans, S. T.; Gokhale, A. A.; Dumesic, J. A.; Mavrikakis, M. Prediction of experimental methanol decomposition rates on platinum from first principles. *Topics in catalysis* **2006**, *37*, 17-28.
- (9) Greeley, J.; Mavrikakis, M. A first-principles study of methanol decomposition on Pt (111). *Journal of the American Chemical Society* **2002**, *124* (24), 7193-7201.
- (10) Greeley, J.; Mavrikakis, M. Competitive paths for methanol decomposition on Pt (111). *Journal of the American Chemical Society* **2004**, *126* (12), 3910-3919.
- (11) Kruse, N.; Rebholz, M.; Matolin, V.; Chuah, G.; Block, J. H. Methanol decomposition on Pd (111) single crystal surfaces. *Surface science* **1990**, *238* (1-3), L457-L462.
- (12) García-Muelas, R.; Li, Q.; Lopez, N. Density functional theory comparison of methanol decomposition and reverse reactions on metal surfaces. *ACS Catalysis* **2015**, *5* (2), 1027-1036.
- (13) Zhou, C.; Ding, D.; Zhu, W.; Chang, X.; Zhang, T.; Wu, H.; Yang, H.; Sun, L. Mechanism of formaldehyde advanced interaction and degradation on Fe<sub>3</sub>O<sub>4</sub> (1 1 1) catalyst: Density functional theory study. *Applied Surface Science* **2020**, *520*, 146324.
- (14) Ma, F.-Q.; Lu, D.-S.; Guo, Z.-Y. Base-catalyzed decomposition of methyl formate to carbon monoxide and methanol over zeolite catalysts. *Journal of molecular catalysis* **1993**, *78* (3), 309-325.
- (15) Liu, Y.; Kirchberger, F. M.; Müller, S.; Eder, M.; Tonigold, M.; Sanchez-Sanchez, M.; Lercher, J. A. Critical role of formaldehyde during methanol conversion to hydrocarbons. *Nature Communications* **2019**, *10* (1), 1462. DOI: 10.1038/s41467-019-09449-7.
- (16) Liu, Y.; Müller, S.; Berger, D.; Jelic, J.; Reuter, K.; Tonigold, M.; Sanchez-Sanchez, M.; Lercher, J. A. Formation Mechanism of the First Carbon–Carbon Bond and the First Olefin in the Methanol

Conversion into Hydrocarbons. *Angewandte Chemie International Edition* **2016**, *55* (19), 5723-5726. DOI: <https://doi.org/10.1002/anie.201511678>.

(17) Jing, W.; Shen, H.; Qin, R.; Wu, Q.; Liu, K.; Zheng, N. Surface and interface coordination chemistry learned from model heterogeneous metal nanocatalysts: from atomically dispersed catalysts to atomically precise clusters. *Chemical Reviews* **2022**, *123* (9), 5948-6002.

(18) Aireddy, D. R.; Ding, K. Heterolytic Dissociation of H<sub>2</sub> in Heterogeneous Catalysis. *ACS Catalysis* **2022**, *12* (8), 4707-4723. DOI: 10.1021/acscatal.2c00584.

(19) Kaithal, A.; Chatterjee, B.; Werlé, C.; Leitner, W. Acceptorless dehydrogenation of methanol to carbon monoxide and hydrogen using molecular catalysts. *Angewandte Chemie International Edition* **2021**, *60* (51), 26500-26505.

(20) Geng, L.; Zhang, M.; Zhang, Z.; Li, Y. Production of carbon monoxide and hydrogen from methanol using a ruthenium pincer complex: a DFT study. *Dalton Transactions* **2023**, *52* (38), 13653-13661, 10.1039/D3DT01912H. DOI: 10.1039/D3DT01912H.

(21) Yang, L.; Guo, X.; Ren, Y.; Gu, R.; Chen, Z.-X.; Zeng, G. Mechanistic Insight into Acceptorless Dehydrogenation of Methanol to Syngas Catalyzed by MACHO-Type Ruthenium and Manganese Complexes: A DFT Study. *Inorganic Chemistry* **2023**, *62* (48), 19516-19526. DOI: 10.1021/acs.inorgchem.3c02619.

(22) Nielsen, M.; Alberico, E.; Baumann, W.; Drexler, H.-J.; Junge, H.; Gladiali, S.; Beller, M. Low-temperature aqueous-phase methanol dehydrogenation to hydrogen and carbon dioxide. *Nature* **2013**, *495* (7439), 85-89.

(23) Alberico, E.; Lennox, A. J. J.; Vogt, L. K.; Jiao, H.; Baumann, W.; Drexler, H.-J.; Nielsen, M.; Spannenberg, A.; Chęcinski, M. P.; Junge, H.; et al. Unravelling the Mechanism of Basic Aqueous Methanol Dehydrogenation Catalyzed by Ru–PNP Pincer Complexes. *Journal of the American Chemical Society* **2016**, *138* (45), 14890-14904. DOI: 10.1021/jacs.6b05692.

(24) Rama, R. J.; Nova, A.; Nicasio, M. C. Microkinetic Model as a Crucial Tool for Understanding Homogeneous Catalysis. *ChemCatChem*, e202400224.

(25) Besora, M.; Maseras, F. Microkinetic modeling in homogeneous catalysis. *Wiley Interdisciplinary Reviews: Computational Molecular Science* **2018**, *8* (6), e1372.

(26) Sciortino, G.; Maseras, F. Microkinetic modelling in computational homogeneous catalysis and beyond. *Theoretical Chemistry Accounts* **2023**, *142* (10), 99.

(27) Konishi, H.; Matsubara, M.; Mori, K.; Tokiwa, T.; Arulmozhiraja, S.; Yamamoto, Y.; Ishikawa, Y.; Hashimoto, H.; Shigeta, Y.; Tokiwa, H.; et al. Mechanistic Insight into Weak Base-Catalyzed Generation of Carbon Monoxide from Phenyl Formate and Its Application to Catalytic Carbonylation at Room Temperature without Use of External Carbon Monoxide Gas. *Advanced Synthesis & Catalysis* **2017**, *359* (20), 3592-3601. DOI: <https://doi.org/10.1002/adsc.201700751>.

(28) Zhao, Y.; Truhlar, D. G. A new local density functional for main-group thermochemistry, transition metal bonding, thermochemical kinetics, and noncovalent interactions. *The Journal of Chemical Physics* **2006**, *125* (19). DOI: 10.1063/1.2370993 (accessed 5/23/2024).

(29) Grimme, S.; Antony, J.; Ehrlich, S.; Krieg, H. A consistent and accurate ab initio parametrization of density functional dispersion correction (DFT-D) for the 94 elements H-Pu. *The Journal of Chemical Physics* **2010**, *132* (15). DOI: 10.1063/1.3382344 (accessed 5/23/2024).

(30) Frisch, M.; Trucks, G.; Schlegel, H.; Scuseria, G.; Robb, M.; Cheeseman, J.; Scalmani, G.; Barone, V.; Petersson, G.; Nakatsuji, H. Gaussian 16, Revision A. 03, Gaussian, Inc., Wallingford CT **2016**, 3.

(31) Weigend, F. Accurate Coulomb-fitting basis sets for H to Rn. *Physical chemistry chemical physics* **2006**, *8* (9), 1057-1065.

(32) Weigend, F.; Ahlrichs, R. Balanced basis sets of split valence, triple zeta valence and quadruple zeta valence quality for H to Rn: Design and assessment of accuracy. *Physical Chemistry Chemical Physics* **2005**, *7* (18), 3297-3305.

(33) Zhao, Y.; Truhlar, D. G. The M06 suite of density functionals for main group thermochemistry, thermochemical kinetics, noncovalent interactions, excited states, and transition elements: two new functionals and systematic testing of four M06-class functionals and 12 other functionals. *Theoretical Chemistry Accounts* **2008**, *120* (1), 215-241. DOI: 10.1007/s00214-007-0310-x.

(34) Marenich, A. V.; Cramer, C. J.; Truhlar, D. G. Universal solvation model based on solute electron density and on a continuum model of the solvent defined by the bulk dielectric constant and atomic surface tensions. *The Journal of Physical Chemistry B* **2009**, *113* (18), 6378-6396.

(35) Troels Skrydstrup, A. B., Joakim Jakobsen et al. Integrating hydroformylations into a methanol economy. **2024**. DOI: <https://doi.org/10.21203/rs.3.rs-4182149/v1>.

(36) Wu, F.; Zhao, Q.; Tao, L.; Danaci, D.; Xiao, P.; Hasan, F. A.; Webley, P. A. Solubility of carbon monoxide and hydrogen in methanol and methyl formate: 298–373 K and 0.3–3.3 MPa. *Journal of Chemical & Engineering Data* **2019**, *64* (12), 5609-5621.